

JOURNAL OF ELECTRONIC MATERIALS

Publisher name: SPRINGER

Journal Impact Factor™

2.1

2022

1.8

Five Year

JCR Category	Category Rank	Category Quartile
ENGINEERING, ELECTRICAL & ELECTRONIC <i>in SCIE edition</i>	179/275	Q3
MATERIALS SCIENCE, MULTIDISCIPLINARY <i>in SCIE edition</i>	249/344	Q3
PHYSICS, APPLIED <i>in SCIE edition</i>	99/160	Q3

Source: Journal Citation Reports 2022. [Learn more](#)

Journal Citation Indicator™

0.41

2022

0.42

2021

JCI Category	Category Rank	Category Quartile
ENGINEERING, ELECTRICAL & ELECTRONIC <i>in SCIE edition</i>	230/352	Q3
MATERIALS SCIENCE, MULTIDISCIPLINARY <i>in SCIE edition</i>	271/424	Q3
PHYSICS, APPLIED <i>in SCIE edition</i>	117/178	Q3

The Journal Citation Indicator is a measure of the average Category Normalized

Full text at publisher



Export

Add To Marked List

Influence of Highly Efficient Carbon Doping on Al_xGa_{1-x}As Layers with Different Al Compositions (x) Grown by MOVPE

By Perkitel, I (Perkitel, Izel) ^{[1], [2]}; Kekuel, R (Kekuel, Reyhan) ^{[1], [2]}; Altuntas, I (Altuntas, Ismail) ^{[1], [2]}; Guer, E (Guer, Emre) ^[3]; Demir, I (Demir, Ilkay) ^{[1], [2]}

[View Web of Science ResearcherID and ORCID](#) (provided by Clarivate)

Source JOURNAL OF ELECTRONIC MATERIALS

Volume: 52 Issue: 9 Page: 6042-6051

DOI: 10.1007/s11664-023-10520-9

Published SEP 2023

Early Access JUN 2023

Indexed 2023-07-16

Document Type Article

Jump to [↓ Enriched Cited References](#)

Abstract Carbon (C)-doped aluminum gallium arsenide (Al_xGa_{1-x}As) epitaxial layers with different aluminum (Al) concentrations have been grown on gallium arsenide (GaAs) substrates by metalorganic vapor phase epitaxy (MOVPE) technique. The impact of varying carbon tetrabromide (CBr₄) flow rates on the electrical properties of Al_xGa_{1-x}As materials with different Al compositions has been investigated. High-resolution x-ray diffraction (HRXRD) measurement and a Hall effect measurement system have been used to determine the Al compositions and to evaluate the electrical properties. It has been found that the carrier density increases and the mobility decreases by increasing the flow rate of CBr₄ and changing Al compositions up to a certain point. In contrast, at higher Al compositions, a decrease in carrier density and an increase in mobility have been observed with increasing CBr₄ flow rate. Since these observed trends require to be analyzed in more detail, x-ray photoelectron spectroscopy (XPS) has been used to analyze the elements in the structure. From the XPS results, it has been shown that the atomic concentration of the arsenic in the structure decreased with the increase in CBr₄ flow rates. In addition, it has been shown that the Al composition in the Al_xGa_{1-x}As material obtained from the XRD results increases with the increase in the atomic concentration of the arsenic. Accordingly, a linear increase in carrier concentration is shown with increasing Al composition. This increase is explained by the effect of the Al-C bond content on the electrical properties of Al(x)Ga(1-x)As.

Citation Network

In Web of Science Core Collec

0 Citations

[Create citation alert](#)

44 Cited References
[View Related Records](#) →

Use in Web of Science

3 Last 180 Days

3 Since 2000

This record is from:

Web of Science Core Collec

- Science Citation Index Exp
- EXPANDED)

Suggest a correction

If you would like to improv



Influence of Highly Efficient Carbon Doping on $\text{Al}_x\text{Ga}_{1-x}\text{As}$ Layers with Different Al Compositions (x) Grown by MOVPE

Izel Perkitel^{1,2} · Reyhan Kekül^{1,2} · Ismail Altuntas^{1,2} · Emre Gür³ · Ilkay Demir^{1,2}

Received: 6 January 2023 / Accepted: 18 May 2023 / Published online: 27 June 2023
© The Minerals, Metals & Materials Society 2023

Abstract

Carbon (C)-doped aluminum gallium arsenide ($\text{Al}_x\text{Ga}_{1-x}\text{As}$) epitaxial layers with different aluminum (Al) concentrations have been grown on gallium arsenide (GaAs) substrates by metalorganic vapor phase epitaxy (MOVPE) technique. The impact of varying carbon tetrabromide (CBr_4) flow rates on the electrical properties of $\text{Al}_x\text{Ga}_{1-x}\text{As}$ materials with different Al compositions has been investigated. High-resolution x-ray diffraction (HRXRD) measurement and a Hall effect measurement system have been used to determine the Al compositions and to evaluate the electrical properties. It has been found that the carrier density increases and the mobility decreases by increasing the flow rate of CBr_4 and changing Al compositions up to a certain point. In contrast, at higher Al compositions, a decrease in carrier density and an increase in mobility have been observed with increasing CBr_4 flow rate. Since these observed trends require to be analyzed in more detail, x-ray photoelectron spectroscopy (XPS) has been used to analyze the elements in the structure. From the XPS results, it has been shown that the atomic concentration of the arsenic in the structure decreased with the increase in CBr_4 flow rates. In addition, it has been shown that the Al composition in the $\text{Al}_x\text{Ga}_{1-x}\text{As}$ material obtained from the XRD results increases with the increase in the atomic concentration of the arsenic. Accordingly, a linear increase in carrier concentration is shown with increasing Al composition. This increase is explained by the effect of the Al–C bond content on the electrical properties of $\text{Al}_x\text{Ga}_{1-x}\text{As}$.

Keywords $\text{Al}_x\text{Ga}_{1-x}\text{As}$ · CBr_4 doping · MOVPE · Al composition

Introduction

III–V compound semiconductors, having a direct band-gap nature, have become one of the most important for photovoltaic and optoelectronic applications and have attracted the great attention of researchers interested in these areas.^{1–7} Especially, among these semiconductor materials, gallium arsenide (GaAs) and aluminum gallium arsenide (AlGaAs) heterostructures can absorb light very efficiently, and thus, they may achieve similar photosensitivity as silicon in considerably smaller quantities, resulting in smaller devices.

Photon-detecting devices based on AlGaAs and GaAs, especially in the visible region, have received considerable attention as viable alternatives to the well-known silicon and germanium-based photodetectors.^{8–11} Also, GaAs and aluminum arsenide (AlAs) are nearly lattice-matched, allowing for the creation of heterostructures from these materials and their alloys with no restrictions on layer thickness or composition.¹² Nowadays, a wide range of devices, such as high-mobility transistors, photodetectors, solar cells, and electro-optical switches, are just some examples of devices made up of $\text{Al}_x\text{Ga}_{1-x}\text{As}/\text{GaAs}$ epitaxial layers.^{13–15} In order to obtain $\text{Al}_x\text{Ga}_{1-x}\text{As}/\text{GaAs}$ epitaxial layers with the desired properties for electronic applications, they should have been grown with adequate purity and high crystalline quality. Electrical properties, optical properties, crystal quality, and thickness control are related to growth techniques. Some of the most successful growth techniques are metalorganic chemical vapor deposition (MOVPE, also called MOCVD), molecular beam epitaxy, and liquid phase epitaxy.

In addition to the advantages that cause this interest in $\text{Al}_x\text{Ga}_{1-x}\text{As}$ based semiconductors, the use of carbon (C)

✉ Ilkay Demir
idemir@cumhuriyet.edu.tr

¹ Nanophotonics Research and Application Center, Sivas Cumhuriyet University, 58140 Sivas, Turkey

² Department of Nanotechnology Engineering, Faculty of Engineering, Sivas Cumhuriyet University, 58140 Sivas, Turkey

³ Department of Physics, Faculty of Science, Eskişehir Osmangazi University, 26040 Eskişehir, Turkey

as a *p*-type dopant in GaAs, and indium gallium arsenide (InGaAs) structures can also provide strong potential with appropriate heterostructure formation. In particular, compared to other *p*-type dopants such as magnesium (Mg), zinc (Zn), and beryllium (Be), C comes forward due to advantages such as less memory effect, low activation energy, higher free hole density, good electrical activity, and high solid solubility.^{16–18} Also, very high doping concentrations 10^{21} cm^{-3} are possible with C due to its low diffusivity.¹⁹ C incorporation can take place using two techniques, unintentional doping (UID) or intentional doping (ID). With a UID carbon process, carbon atoms from the group III precursor can be incorporated into the growing material by lowering the V/III ratio and growth temperature.^{20–22} In terms of growth, it is unsuitable for quickly changing the V/III ratio and temperature of superlattices with hundreds of thin layers from one layer to another.²³ On the other hand, the carbon doping concentration can be controlled by UID without changing the V/III ratio and growth temperature.²⁴ In III–V semiconductors, carbon is of interest as an intentional acceptor due to some of its physical properties. The use of ID sources has allowed the development of MOVPE device applications.²⁵ Halomethanes such as carbon tetrachloride (CCl₄), carbon tetrabromide (CBr₄), and carbon bromide chloride (CBrCl₃) are used for ID carbon since high doping efficiency can be achieved due to weak C–Cl or C–Br bonds.^{26,27} C-doped AlGaAs/GaAs can be produced by using extrinsic doping precursors such as carbon tetrabromide (CBr₄) and carbon tetrachloride (CCl₄).²⁸ The advantage of using CBr₄ is that the growth conditions are more flexible to reach the desired doping level without compromising other material properties.¹⁴ Another use for CBr₄ is the in situ etching of AlGaAs. Andre et al. studied in situ etching of Al_xGa_{1-x}As in MOVPE using CBr₄. They showed that, while the etch rate was almost constant for GaAs at temperatures of 600°C and 700°C, it decreased markedly at higher temperatures with higher Al compositions.²⁹ In the literature, some studies have explained the relationship between the Al composition and the doping rate of Al_xGa_{1-x}As. In this context, Kakinuma et al. showed that there is a linear relationship between *x* and the doping rate in a study discussing UID carbon composition.³⁰ However, Fujii et al. and Kuech et al. have reported that this relationship is in the form of a square. The higher V/III ratio leads to a lower carbon concentration, which is fundamentally the same tendency as in the GaAs case. The carbon concentration usually decreases with increasing growth temperature, and this trend is affected by the arsine (AsH₃) mole fraction.^{31,32} Also, in other studies where CCl₄²⁶ and tertiary butylarsine (TBAs)³³ were used as doping sources, a marked carbon increase was obtained in the *x* composition of Al_xGa_{1-x}As between 0.5 and 0.7, while an almost constant carbon ratio was obtained in higher *x* compositions.³⁴ These

studies which discussed the relationship between Al concentration and doping level just explain a uniform relationship. Moreover, to our knowledge, there is no study showing the effect of the variation of the CBr₄ flow on the doping level and Al concentration in structures with high Al content.

A deeper knowledge of the consequences of Al composition in enhancing doping precursor flows and different Al concentrations in Al_xGa_{1-x}As alloy is therefore critical before its integration into opto-electronic devices. In this study, we focus on the carbon doping effect on the carrier density of Al_xGa_{1-x}As with changing the Al concentration. Therefore, successfully grown high-quality Al_xGa_{1-x}As epitaxial layers are studied here in detail by high-resolution x-ray diffraction (HRXRD), the Hall effect measurement system (HEMS), and x-ray photoelectron spectroscopy (XPS).

Experimental

Al_xGa_{1-x}As structures have been grown on a GaAs (001) substrate by an AIXTRON 200/4 RF-S MOVPE system. The metal–organic compounds trimethylgallium (TMGa) and trimethylaluminum (TMAI) have been used as gallium and aluminum precursors, respectively. The GaAs buffer layer has been grown at ~ 25 nm thickness and the reactor temperature and pressure during growth of the buffer layer have been kept constant at 690°C and 100 mbar, respectively. This buffer layer has been grown under the same conditions for all the samples with a TMGa flow of $6.3 \times 10^1 \mu\text{mol/min}$ and an AsH₃ flow of $1.3 \times 10^3 \mu\text{mol/min}$. After the buffer layer growth, the reactor temperature was increased from 690°C to 730°C, and Al_xGa_{1-x}As structures with different Al compositions were grown. All the other parameters have been kept constant except for the CBr₄ flow rate of the samples grown in four different groups. The group A samples have been grown with a TMAI flow of $1.8 \mu\text{mol/min}$, a TMGa flow of $6.7 \times 10^1 \mu\text{mol/min}$, and an AsH₃ flow of $8.9 \times 10^2 \mu\text{mol/min}$ and contains 4 different samples. The CBr₄ flow rates are $2.3 \mu\text{mol/min}$, $4.6 \mu\text{mol/min}$, $6.9 \mu\text{mol/min}$, and $9.2 \mu\text{mol/min}$ for samples A1, A2, A3, and A4, respectively. The intended layer thickness for Group A is ~ 350 nm. The Group B samples have been grown with TMAI flow of $8.8 \mu\text{mol/min}$, a TMGa flow of $4.5 \times 10^1 \mu\text{mol/min}$, and an AsH₃ flow of $8.9 \times 10^2 \mu\text{mol/min}$ and contains 3 different samples. The CBr₄ flow rates are $1.5 \mu\text{mol/min}$, $2.3 \mu\text{mol/min}$, and $4.6 \mu\text{mol/min}$ for samples B1, B2, and B3, respectively. The intended layer thickness for Group B is ~ 250 nm (~ 350 nm for B1). The Group C samples have been grown with a TMAI flow of $6.6 \mu\text{mol/min}$, a TMGa flow of $8.9 \mu\text{mol/min}$, and an AsH₃ flow of $8.9 \times 10^2 \mu\text{mol/min}$ and contains 2 different samples. The CBr₄ flow rates are $1.0 \mu\text{mol/min}$, and $1.5 \mu\text{mol/min}$ for samples C1 and

C2, respectively. The intended layer thickness for Group C is ~ 250 nm. The Group D samples have been grown with a TMAI flow of $3.3 \times 10^1 \mu\text{mol}/\text{min}$, a TMGa flow of $8.9 \mu\text{mol}/\text{min}$, and an AsH_3 flow of $8.9 \times 10^2 \mu\text{mol}/\text{min}$ and contains 3 different samples. The CBr_4 flow rates are $1.0 \mu\text{mol}/\text{min}$, $2.4 \mu\text{mol}/\text{min}$, and $8.1 \mu\text{mol}/\text{min}$ for samples D1, D2, and D3, respectively. The intended layer thickness for Group D is ~ 280 nm. Figure 1 shows a schematic of the grown AlGaAs layers, while the growth parameters and the Al composition (%) values are summarized in Table I.

Results and Discussion

The properties of the material we have produced have an active role in the behavior of semiconductor devices. Thus, the performance of semiconductor devices depends on the quality of the material, and many techniques are used to determine the structural, electrical, and optical qualities. The x-ray diffraction (XRD) technique, the most basic technique

that does not damage the material, is used to determine the alloy ratios and lattice constants of ternary alloys, the structural characteristics, and the quality of semiconductor thin films. XRD also allows us to obtain important information in sub-nanometer orders: the thickness of epitaxial layers, the chemical composition of materials, lattice strains, and the density of the dislocations.^{35–38} In this study, a θ - 2θ scan by using the XRD system (the wavelength of the x-ray used was $\lambda_{\text{CuK}\alpha} = 0.15405$ nm) has been performed to determine the alloy ratios and lattice constants of the samples. After the XRD scans, both the thicknesses and alloy ratios of the grown layers have been obtained with the help of the GlobalFit simulation software developed by Rigaku. The simulations and XRD measurements of A1, B1, C1, and D1 are shown in Fig. 2. In these graphs, red, blue, green, and purple lines correspond to the XRD measurement results and the black line represents the simulation results. As can be clearly seen in Fig. 2, the simulation and the XRD measurement results overlap very well. Excellent compatibility between simulation and measurement is essential to obtain

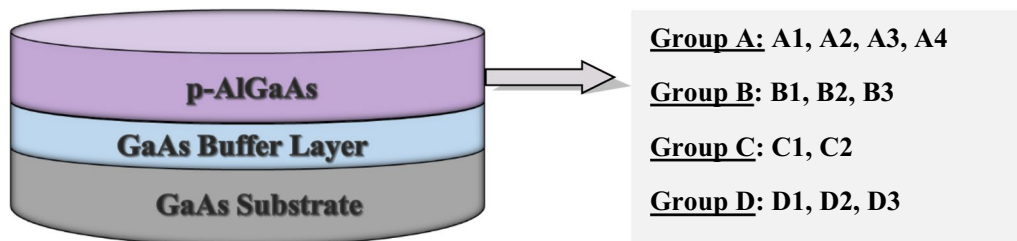


Fig. 1 Schematic of AlGaAs samples.

Table I Growth parameters of samples grown via MOVPE and Al compositions (%) and thickness values from XRD

Group	T ($^{\circ}\text{C}$)	TMAI ($\mu\text{mol}/\text{min}$)	TMGa ($\mu\text{mol}/\text{min}$)	AsH_3 ($\mu\text{mol}/\text{min}$)	CBr_4 ($\mu\text{mol}/\text{min}$)	Al %	Thickness (nm)
<i>Group A</i>							
A1	730	1.8	6.7×10^1	8.9×10^2	2.3	6	340
A2	730	1.8	6.7×10^1	8.9×10^2	4.6	6	358
A3	730	1.8	6.7×10^1	8.9×10^2	6.9	6	345
A4	730	1.8	6.7×10^1	8.9×10^2	9.2	6	354
<i>Group B</i>							
B1	730	8.8	4.5×10^1	8.9×10^2	1.5	34	360
B2	730	8.8	4.5×10^1	8.9×10^2	2.3	34	242
B3	730	8.8	4.5×10^1	8.9×10^2	4.6	34	240
<i>Group C</i>							
C1	730	6.6	8.9	8.9×10^2	1.0	64	255
C2	730	6.6	8.9	8.9×10^2	1.5	64	235
<i>Group D</i>							
D1	730	3.3×10^1	8.9	8.9×10^2	1.0	92.7	284
D2	730	3.3×10^1	8.9	8.9×10^2	2.4	92.1	276
D3	730	3.3×10^1	8.9	8.9×10^2	8.1	88.7	280

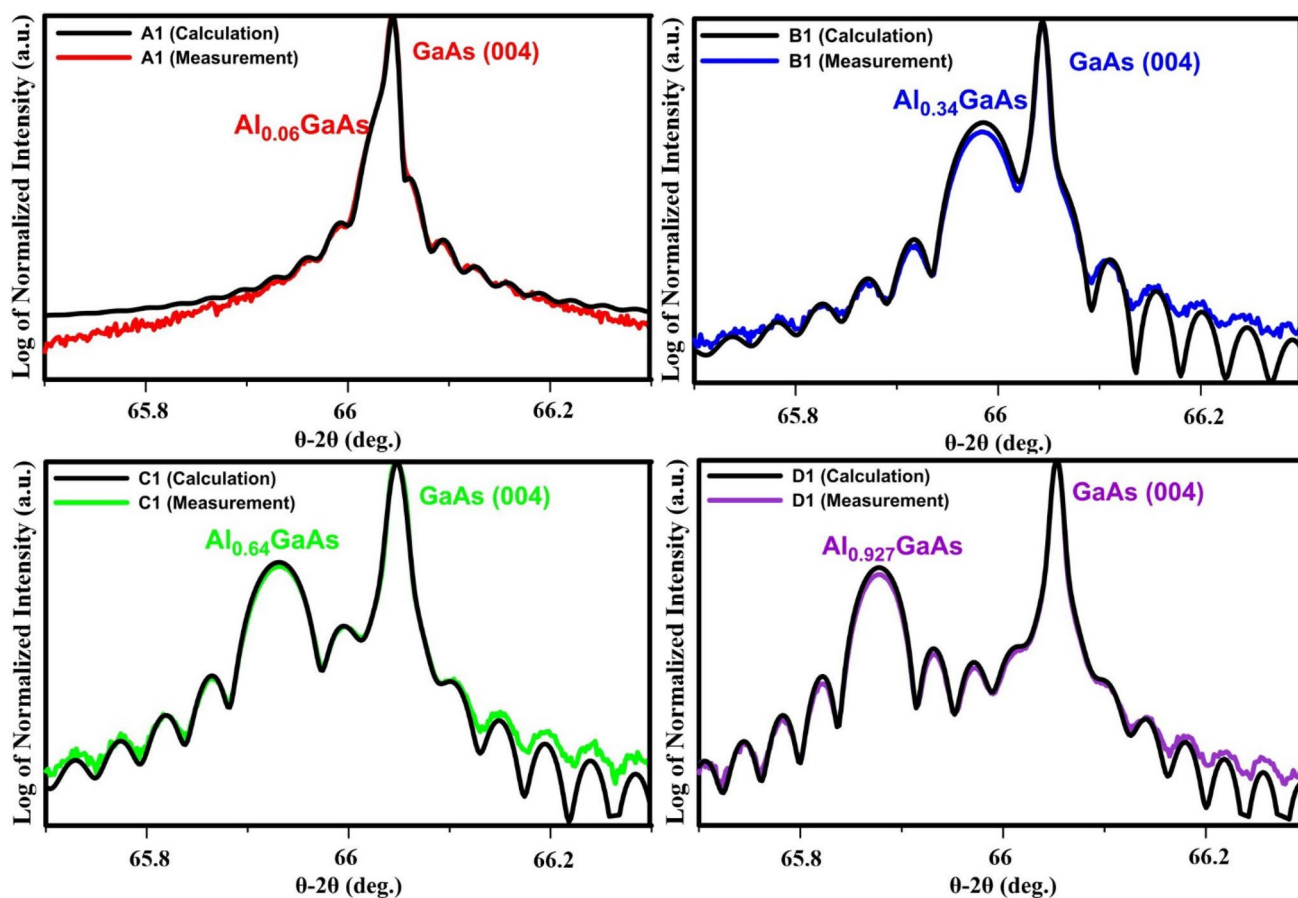


Fig. 2 Simulation and XRD measurements for samples A1, B1, C1, and D1. The red, blue, green, and purple lines represent the XRD measurement results, the black line corresponds to the simulation (Color figure online)

comprehensive and accurate information from the grown samples.

Figure 3 shows the θ - 2θ scans of the Group A, B, C, and D samples. The Al_xGa_{1-x}As peak and the GaAs (004) peak intertwine due to the low Al content for Group A, although the diffraction peak of the GaAs (004) substrate on the right and the Al_xGa_{1-x}As peak on the left is clearly seen for Groups B, C, and D. The diffraction peak shifts to smaller angles for the Al_xGa_{1-x}As layers with increasing Al compositions. The diffraction peaks of Al_xGa_{1-x}As for Groups A, B, C, and D can be seen at angles of approximately 66.03°, 65.98°, 65.92°, and 65.87–65.88°, respectively. Using the GlobalFit simulation software as shown in Fig. 2, the Al concentrations corresponding to these diffraction angles for Groups A, B, C, and D have been obtained as 0.06, 0.34, 0.64, and 0.927–0.887, respectively. When the XRD results for the Al concentrations obtained in the Group D samples have been examined in detail, a lower Al concentration (0.921) has been obtained for the D2 sample, which has approximately 2.5 times more CBr₄ flow rate than that used in the D1 sample under the same growing conditions. Likewise, a lower Al concentration (0.887) has been obtained

when the CBr₄ flow rate is increased by approximately 3.5 times in the D3 sample compared to the D2 sample. The findings demonstrate that CBr₄ flow has an influence on the Al concentration in the Al_xGa_{1-x}As samples with high Al content.

More information using the XRD results can be obtained about the grown samples. As is well known, the x-rays of the crystal planes interact with the atoms in the periodic plane, and the diffraction pattern formed as a result of this interaction is explained by Bragg's law³⁹:

$$2d \sin \theta = n\lambda \quad (1)$$

where λ corresponds to the wavelength of the x-ray used, d is the distance between the lattice planes, n is the order of reflection, and θ stands for the Bragg angle. The distance between the lattice planes for cubic crystal systems is given by⁴⁰:

$$d_{hkl} = \frac{a}{\sqrt{h^2 + k^2 + l^2}} \quad (2)$$

where a is the lattice constant and integers h , k , and l correspond to the Miller indices.

Also, Vegard's law gives the relationship between a ternary alloy and binary compounds and is given by⁴¹:

$$a_{\text{Al}_x\text{Ga}_{1-x}\text{As}} = xa_{\text{AlAs}} + (1-x)a_{\text{GaAs}} \quad (3)$$

where x and $(1-x)$ are the ratio of AlAs and GaAs compounds in the ternary alloy, respectively. The lattice parameters of AlAs and GaAs compounds are 5.66139 Å and 5.65330 Å, respectively.⁴² According to Vegard's law, the lattice parameter (a_0) can be calculated by using the Al

composition (x) of the $\text{Al}_x\text{Ga}_{1-x}\text{As}$ layer obtained from the result of the XRD measurement. The a_0 values have been obtained as 5.6560 Å for the Group B samples, 5.6584 Å for the Group C samples, and 5.6608 Å, 5.6607 Å, and 5.6605 Å for the D1, D2, and D3 samples, respectively.

In order to calculate the strain, the reference a_0 value is defined and the following expression is used^{37,38}:

$$\varepsilon_a = \frac{a_{\text{measured}} - a_0}{a_0} \quad (4)$$

where ε_a stands for strain.

Both the lattice parameters (a) and the strain values (ε_a) for all the samples have been calculated, and the results are given in Table II. The lattice parameters and strain values for samples A1, A2, A3, and A4 could not be calculated due to the unclear position of the diffraction angle (θ) of the $\text{Al}_x\text{Ga}_{1-x}\text{As}$.

The increase in Al composition from 0.34 to 0.927 of the $\text{Al}_x\text{Ga}_{1-x}\text{As}$ epilayers causes a rise in the strain ratios and lattice parameters due to the lattice mismatch between the epilayers and the substrate.

The electrical characterization of $\text{Al}_x\text{Ga}_{1-x}\text{As}$ structures grown on the GaAs substrate via HEMS has been examined. Figure 4a, b, c, and d shows the variation of Hall mobility and carrier density values with the changing of CBr_4 flow for Groups A, B, C, and D, respectively. As can be seen from Fig. 4a, b, and c, the carrier density increases and the mobility decreases as the flow rate of CBr_4 increases. Since the variation in the CBr_4 flow rate triggers the formation of some scattering mechanisms, it causes changes in both carrier density and mobility values. Alloy scattering, impurity scattering, and interface roughness scattering mostly lead to reduced mobility. Also, the relationship between the mobility $\mu(al)$ and alloy content is given by Eq. 5, with mobility value depending on the mole fraction x (alloy scattering)⁴³:

$$\mu(al) \propto \frac{1}{x(1-x)} \quad (5)$$

The variation of CBr_4 flow rate on the carrier density and mobility have a similar impact for Groups A, B, and C. However, in contrast to the behavior for Groups A, B, and C, the variation of the CBr_4 flow rate causes an inverse effect for Group D, as shown in Fig. 4d.

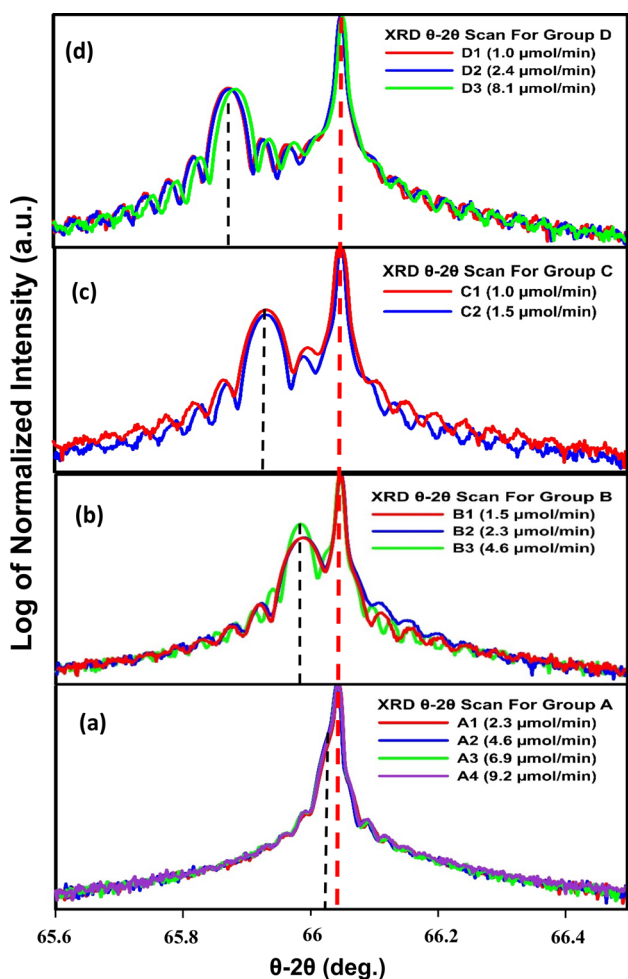


Fig. 3 XRD θ - 2θ scans of Group A (a), Group B (b), Group C (c), and Group D (d).

Table II Lattice parameters (a) and strain rates of Groups B, C, and D

	Group B			Group C		Group D		
	B1	B2	B3	C1	C2	D1	D2	D3
a (Å)	5.6565	5.6555	5.6565	5.6605	5.6606	5.6648	5.6647	5.664
Strain (%)	0.0076	0.0097	0.0075	0.036	0.038	0.071	0.069	0.063

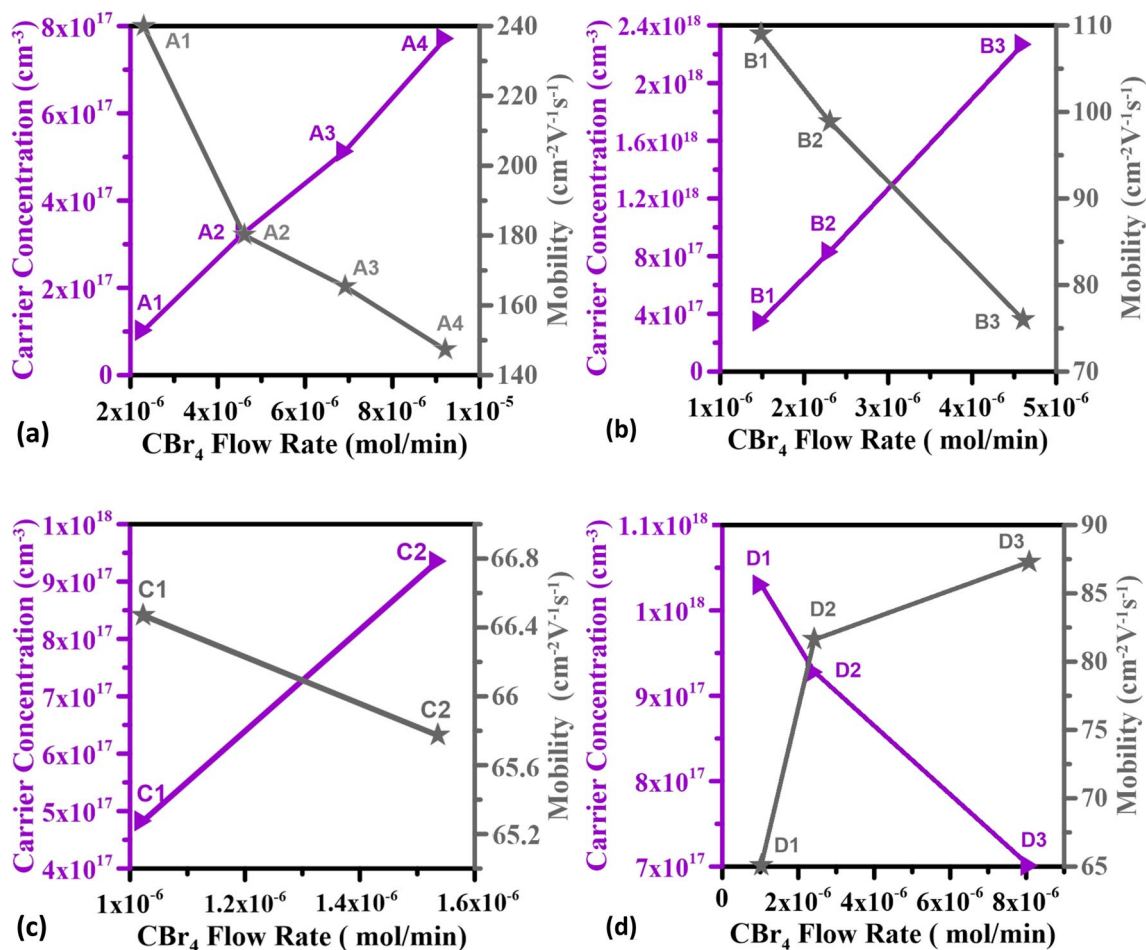


Fig. 4 The effect of CBr₄ flow rate on the carrier density and mobility values of Group A (a), Group B (b), Group C (c), and Group D (d).

The sheet resistance is also one of the electrical characterization parameters. Figure 5 shows the effect of the CBr₄ flow rate on the sheet resistance of the Al_xGa_{1-x}As epilayer. The sheet resistance is defined by⁴⁴:

$$R_{sq} = \frac{1}{e\mu Nd} \tag{6}$$

where R_{sq} , e , μ , N , and d correspond to the sheet resistance, the electron charge, carrier mobility, carrier concentration, and film thickness, respectively. If the film thickness is kept fixed, the layer resistance R_{sq} varies with both the carrier density and the mobility.

The sheet resistance varies inversely proportional to the flow rate of CBr₄ for Groups A, B, and C due to the linear relationship between both carrier density and mobility values with the CBr₄ flow rate. The reason for this can be easily understood from Eq. 6. As previously mentioned for these samples, an increased CBr₄ flow rate led to an increase in carrier density and a decrease in mobility. These variations in the carrier density and mobility result

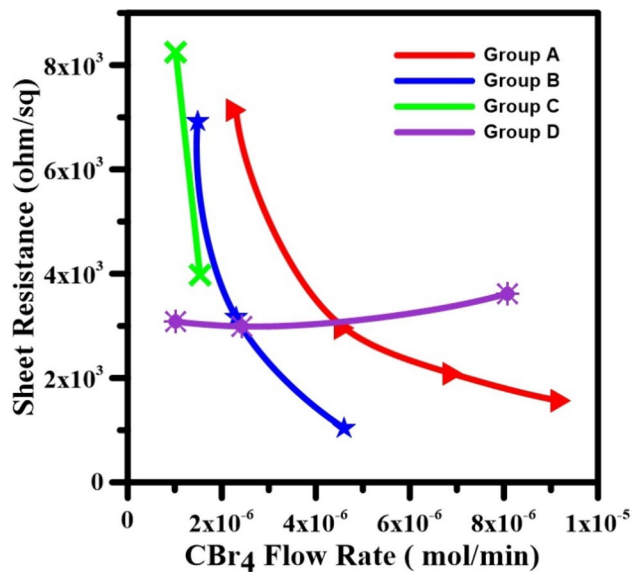


Fig. 5 Variation of sheet resistance as a function of CBr₄ flow rate for Groups A, B, C, and D.

in a reduction in the sheet resistance for Groups A, B, and C. In contrast, the sheet resistance tends to increase slightly due to the decrease in carrier density and increase in mobility with increasing CBr_4 flow rate for Group D. It can be seen that the D3 sample with the highest CBr_4 flow rate has the highest sheet resistance.

The change in Al composition (x) and carrier concentration caused by the CBr_4 flow rate in the $\text{Al}_x\text{Ga}_{1-x}\text{As}$ material has to be investigated by further analysis. Therefore, $\text{Al}_x\text{Ga}_{1-x}\text{As}$ materials in Group D with different CBr_4 flow rates have been analyzed by XPS. Figure 6 shows the XPS spectra of the D1, D2, and D3 samples. It has also been shown that elements such as Al, Ga, As, C, and O have been obtained from AlGaAs films, with the O and C elements due to surface contamination. It can be seen from the figure that there is no significant chemical shift in the elements observed for $\text{Al}_x\text{Ga}_{1-x}\text{As}$ grown at different CBr_4 flow rates, and that the elements observed in the sample are the same. As a result of this, the variation of the CBr_4 flow rate does not reveal other types of impurities.

Figure 7a shows the normalized atomic concentration of the arsenic obtained from wide range XPS spectra plots versus varying CBr_4 flow rates. It has been observed that the atomic concentration of the As in the structure decreases with the increase in CBr_4 flow rates. As a p -type dopant, C is incorporated into the As site in AlGaAs.^{1,17} With increasing CBr_4 flow rate, more C atoms may have preferred to occupy more As sites. For this reason, sample D3 has the least atomic concentration of As with the highest CBr_4 flow

rate. In addition, Fig. 7b shows that the Al composition x in the $\text{Al}_x\text{Ga}_{1-x}\text{As}$ material obtained from the XRD results increases with the increase in the atomic concentration of the As. Considering the growth parameters for the samples in Group D, Table I shows that the TMAI and TMGa flow rates are $3.3 \times 10^1 \mu\text{mol}/\text{min}$ and $8.9 \mu\text{mol}/\text{min}$, respectively. That is, these samples have a quite high Al content. Therefore, it is thought that the probability of Al–As bonding increases with the increase of arsine atoms in the structure. In conclusion, Fig. 7c shows the relationship between Al composition x and carrier concentration in the $\text{Al}_x\text{Ga}_{1-x}\text{As}$ layer. There is a linear increase in carrier concentration with increasing aluminum fraction. This increase can be explained by the effect of the Al–C bond content on the electrical properties of $\text{Al}_x\text{Ga}_{1-x}\text{As}$. In other words, sample D1 with the highest Al composition (92.7%) has more Al–C bond content and, accordingly, the highest carrier density value ($1.03 \times 10^{18} \text{ cm}^{-3}$).

Conclusions

The electrical and structural properties of $\text{Al}_x\text{Ga}_{1-x}\text{As}$ epitaxial layers with different Al concentrations and different CBr_4 flow rates have been investigated by XRD, HEMS, and XPS characterizations. HRXRD results show that the increase in Al composition ($x = 0.34$ – 0.927) of the $\text{Al}_x\text{Ga}_{1-x}\text{As}$ epilayers resulted in an increase in strain ratios from 0.0075% to 0.071% and lattice parameters from

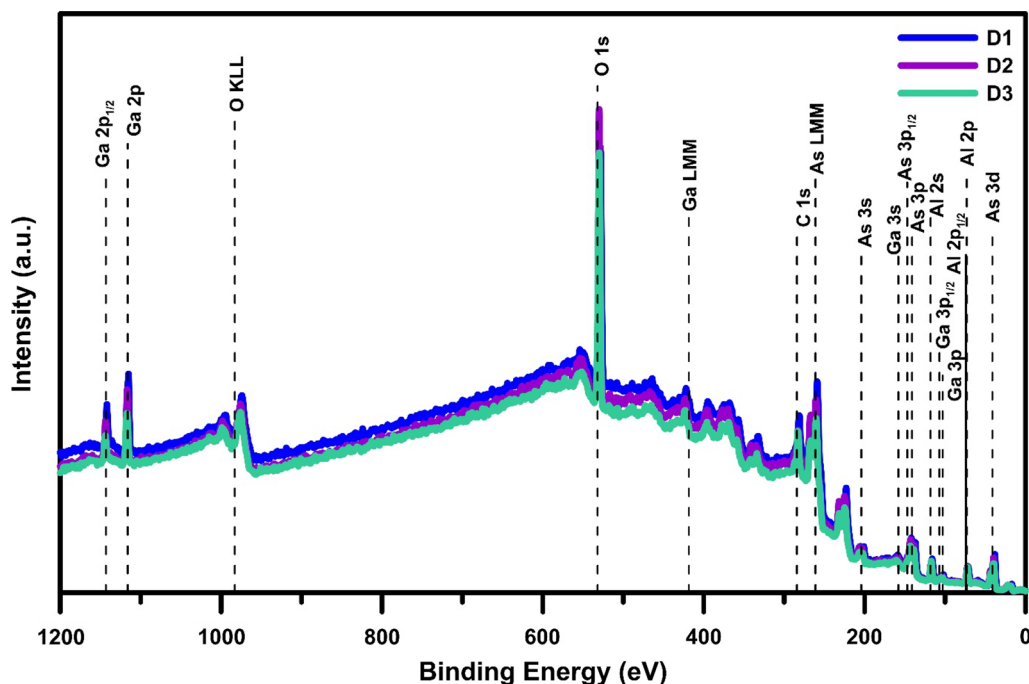


Fig. 6 Wide energy range XPS spectra of D1, D2, and D3 samples.

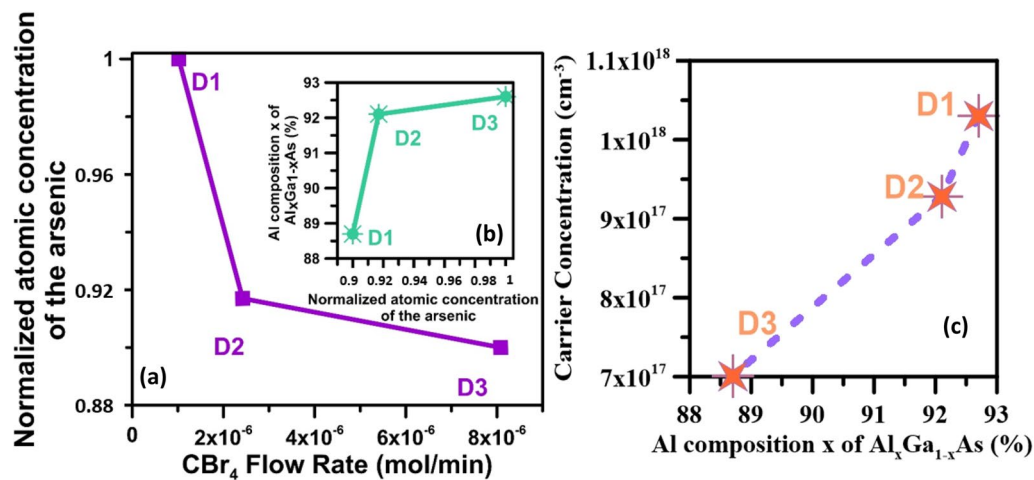


Fig. 7 Normalized atomic concentration of the arsenic from the XPS spectrum versus CBr_4 flow rate (a), Al composition (x) in $\text{Al}_x\text{Ga}_{1-x}\text{As}$ material versus normalized atomic concentration of the arsenic (b),

and carrier concentration versus Al composition (x) in $\text{Al}_x\text{Ga}_{1-x}\text{As}$ material (c).

5.6555 Å to 5.6648 Å due to lattice mismatch between the epilayers and the substrate. Also, it has been seen that an increase in carrier concentration and a decrease in mobility take place by enhancing the CBr_4 flow for different Al concentrations up to a critical point. Moreover, the sheet resistance results reveal that the critical point results from a high Al concentration with the variation of CBr_4 flow rate in the $\text{Al}_x\text{Ga}_{1-x}\text{As}$ layers. In addition, it has been observed that the high amount of both Al and the CBr_4 flow rate affected the Al concentration in the structure, and the reason for this has been explained using the atomic concentration of the arsenic from the XPS results for Group D. It has been shown that the atomic concentration of the arsenic in the structure decreases with the increase in CBr_4 flow rates. From this result, it is predicted that, with an increasing CBr_4 flow rate, more carbon atoms may have preferred to occupy more As sites. The Al composition x in the $\text{Al}_x\text{Ga}_{1-x}\text{As}$ material obtained from the XRD results shows that it increases with the increase in the atomic concentration of the arsenic. Since these samples have very high Al contents, it is thought that the probability of the Al–As bond increases with the increase of arsine atoms in the structure. As a result, there is a linear increase in carrier concentration with increasing aluminum fraction. That is, the D1 sample with the highest Al composition has more Al–C bond content and accordingly the highest carrier density value. Our research yields recent insights into the grasping of the structural and electrical responses in C-doped $\text{Al}_x\text{Ga}_{1-x}\text{As}$ with different Al compositions.

Acknowledgments This study is supported by TUBITAK under Project Number 116F365 and by the Scientific Research Project Fund of Sivas

Cumhuriyet University under the Project Number MRK-2022-003. The authors acknowledge the usage of the Nanophotonics Research and Application Center at Sivas Cumhuriyet University (CUNAM) facilities.

Conflict of interest The authors declare that they have no conflict of interest.

References

1. Z. He, H. Wang, Q. Wang, J. Fan, Y. Zou, and X. Ma, The effect of unintentional carbon incorporation on the electrical properties of AlGaAs grown by MOCVD. *Opt. Mater.* 108, 110227 (2020).
2. C.C. Hou, H.M. Chen, J.C. Zhang, N. Zhuo, Y.Q. Huang, R.A. Hogg, D.T.D. Childs, J.Q. Ning, Z.G. Wang, F.Q. Liu, and Z.Y. Zhang, Near-infrared and mid-infrared semiconductor broadband light emitters. *Light Sci. Appl.* 7(3), 17170 (2018).
3. T. Hidouri, F. Saidi, H. Maaref, Ph. Rodriguez, and L. Auvray, LSE investigation of the thermal effect on band gap energy and thermodynamic parameters of BInGaAs/GaAs single quantum well. *Opt. Mater.* 62, 267 (2016).
4. K.M. Pürü, M.N. Koçak, G. Yolcu, İ Perkitel, İ Altuntaş, and I. Demir, Growth and characterization of PALE Si-doped AlN on sapphire substrate by MOVPE. *Mater. Sci. Semicond. Process.* 142, 106464 (2022).
5. I. Altuntas, M.N. Kocak, G. Yolcu, H.F. Budak, A.E. Kasapoğlu, S. Horoz, E. Gür, and I. Demir, Influence of the PALE growth temperature on quality of MOVPE grown AlN/Si (111). *Mater. Sci. Semicond. Process.* 127, 105733 (2021).
6. I. Simsek, G. Yolcu, M.N. Koçak, K. Pürü, I. Altuntas, and I. Demir, Nucleation layer temperature effect on AlN epitaxial layers grown by metalorganic vapour phase epitaxy. *J. Mater. Sci. Mater. Electron.* 32, 25507 (2021).
7. İ Perkitel, İ Altuntas, and İ Demir, The effect of Si (111) substrate surface cleaning on growth rate and crystal quality of MOVPE grown AlN. *Gazi Univ. J. Sci.* 35(1), 281 (2021).
8. R. Jayaprakash, K. Georgiou, H. Coulthard, A. Askitopoulos, S.K. Rajendran, D.M. Coles, A.J. Musser, J. Clark, I.D.W.

- Samuel, G.A. Turnbull, P.G. Lagoudakis, and D.G. Lidzey, A hybrid organic–inorganic polariton LED. *Light Sci. Appl.* 8(1), 81 (2019).
9. H.Y. Lu, S.C. Tian, C.Z. Tong, L.J. Wang, J.M. Rong, C.Y. Liu, H. Wang, S.L. Shu, and L.J. Wang, Extracting more light for vertical emission: high power continuous wave operation of 1.3- μm quantum-dot photonic-crystal surface-emitting laser based on a flat band. *Light Sci. Appl.* 8(1), 108 (2019).
 10. I. Demir, A.E. Kasapoğlu, H.F. Budak, E. Gür, and S. Elagoz, Influences of thickness and temperature of low temperature GaAs buffer layer on two-step MOVPE grown GaAs/Ge heterostructures. *Eur. Phys. J. Appl. Phys.* 90(2), 20301 (2020).
 11. I. Demir, The contribution of AsH₃: pre-flow and V/III ratio effects on heteroepitaxially grown GaAs/Ge. *Superlattices Microstruct.* 128, 1 (2019).
 12. C. Gerl, S. Schmult, H.P. Tranitz, C. Mitzkus, and W. Wegscheider, Carbon-doped symmetric GaAs/AlGaAs quantum wells with hole mobilities beyond 10⁶ cm²/V s. *Appl. Phys. Lett.* 86(25), 252105 (2005).
 13. J.D. Reyes, R.C. Ojeda, M.G. Arellano, and R.P. Sierra, Raman and Hall characterization of AlGaAs epilayers grown by MOCVD using elemental arsenic. *Superf. Vacío* 15, 22 (2002).
 14. T. Lee, H. Rho, J.D. Song, and W.J. Choi, Raman scattering from GaAs/AlGaAs multiple quantum well structures grown by two-step molecular beam epitaxy. *Curr. Appl. Phys.* 17(3), 398 (2017).
 15. C.D. Noorzad, X. Zhao, V. Harotoonian, and J.M. Woodall, Improved high-energy response of AlGaAs/GaAs solar cells using a low-cost technology. *J. Electron. Mater.* 45, 6317 (2016).
 16. H. Li, F. Reinhardt, L. Birch, and G. Bradford, High-efficient carbon-doped InGaAs/AlGaAs/GaAs quantum well lasers. *J. Cryst. Growth* 263(1–4), 181 (2004).
 17. H.Q. Hou, Carbon doping and etching of Al_xGa_{1-x}As (0 ≤ x ≤ 1) with carbon tetrachloride in metalorganic vapor phase epitaxy. *Appl. Phys. Lett.* 70(26), 3600 (1997).
 18. P. Lian, T. Yin, Z.T. Xu, H. Zhao, D. Zou, G. Gao, J. Du, C. Chen, C. Tao, J. Chen, G. Shen, Q. Cao, X. Ma, and L. Chen, High-quality carbon-doped GaAs/AlGaAs material growth in MOCVD and its application for optoelectronic devices. *Semicond. Lasers III* 3547, 278 (1998).
 19. S. Cho, and E.K. Kim, Band gap narrowing effects in carbon doped GaAs by photoluminescence spectroscopy. *Proc. IEEE* 2, 1099 (1999).
 20. M. Konagai, T. Yamada, T. Akatsuka, K. Saito, E. Tokumitsu, and K. Takahashi, Metallic p-type GaAs and GaAlAs grown by metalorganic molecular beam epitaxy. *J. Cryst. Growth* 98(1–2), 167 (1989).
 21. N. Watanabe, H. Ito, and T. Ishibashi, Carbon doping in GaAs using trimethylarsine by metalorganic chemical vapor deposition with high-speed rotating susceptor. *J. Cryst. Growth* 147(3–4), 256 (1995).
 22. M. Pristovsek, B. Han, J.T. Zettler, and W. Richter, In situ investigation of GaAs (001) intrinsic carbon p-doping in metalorganic vapour phase epitaxy. *J. Cryst. Growth* 221(1–4), 149 (2000).
 23. I. Demir, and S. Elagoz, Interruption time effects on InGaAs/InAlAs superlattices of quantum cascade laser structures grown by MOCVD. *Superlattices Microstruct.* 100, 723 (2016).
 24. C.Z. Kim, H. Kim, K.M. Song, D.H. Jun, H.K. Kang, W. Park, and C.G. Ko, Enhanced efficiency in GaInP/GaAs tandem solar cells using carbon doped GaAs in tunnel junction. *Microelectron. Eng.* 87(4), 677 (2010).
 25. T.F. Kuech, and J. Redwing, Carbon doping in metalorganic vapor phase epitaxy. *J. Cryst. Growth* 145(1–4), 382 (1994).
 26. J.S. Lee, I. Kim, B.D. Choe, and W.G. Jeong, Carbon doping and growth rate reduction by CCl₄ during metalorganic chemical-vapor deposition of GaAs. *J. Appl. Phys.* 76(9), 5079 (1994).
 27. F. Brunner, T. Bergunde, E. Richter, P. Kurpas, M. Achouche, A. Maaßdorf, J. Würfl, and M. Weyers, Carbon doping for the GaAs base layer of heterojunction bipolar transistors in a production scale MOVPE reactor. *J. Cryst. Growth* 221(1–4), 53 (2000).
 28. R.S. Castillo-Ojeda, J. Díaz-Reyes, M.G. Arellano, M.C. Peralta-Clara, and J.S. Veloz-Rendón, Growth and characterization of Al_xGa_{1-x}As obtained by metallic-arsenic-based-MOCVD. *Mater. Res.* 20, 1166 (2017).
 29. A. Maaßdorf, and M. Weyers, In-situ etching of GaAs/Al_xGa_{1-x}As by CBr₄. *J. Cryst. Growth* 310(23), 4754 (2008).
 30. H. Kakinuma, M. Mohri, and M. Akiyama, Characterization of oxygen and carbon in undoped AlGaAs grown by organometallic vapor-phase epitaxy. *Jpn. J. Appl. Phys.* 36(1R), 23 (1997).
 31. K. Fujii, M. Satoh, K. Kawamura, and H. Gotoh, Dependence of carbon incorporation on growth conditions for unintentionally doped AlGaAs during metalorganic vapor-phase epitaxy. *J. Cryst. Growth* 204(1–2), 10 (1999).
 32. T.F. Kuech, D.J. Wolford, E. Veuhoff, V. Deline, P.M. Mooney, R. Potemski, and J. Bradley, Properties of high-purity Al_xGa_{1-x}As grown by the metalorganic vapor-phase-epitaxy technique using methyl precursors. *J. Appl. Phys.* 62(2), 632 (1987).
 33. S. Leu, F. Höhnsdorf, W. Stolz, R. Becker, A. Salzmann, and A. Greiling, C- and O-incorporation in (AlGa) As epitaxial layers grown by MOVPE using TBAs. *J. Cryst. Growth* 195(1–4), 98 (1998).
 34. J. Van Deelen, G.J. Bauhuis, J.J. Schermer, and P.K. Larsen, Parameter study of intrinsic carbon doping of Al_xGa_{1-x}As by MOCVD. *J. Cryst. Growth* 271(3–4), 376 (2004).
 35. H. Fitouri, M.M. Habchi, and A. Rebey, High-resolution X-ray diffraction of III–V semiconductor thin films, *X-Ray Scattering*. ed. A.E. Ares (Rijeka: InTech, 2017), p. 159.
 36. J. Singh, *Electronic and Optoelectronic Properties of Semiconductor Structures* (Cambridge: Cambridge University Press, 2007).
 37. A.K. Bilgili, Ö. Akpınar, G. Kurtulus, M.K. Ozturk, S. Ozcelik, and E. Ozbay, Structural properties of InGaN/GaN/Al₂O₃ structure from reciprocal space mapping. *J. Mater. Sci. Mater. Electron.* 29, 12373 (2018).
 38. B. Smiri, M.B. Arbia, D. Ilkay, F. Saidi, Z. Othmen, B. Dkhil, A. Ismail, E. Sezai, F. Hassen, and H. Maaref, Optical and structural properties of In-rich In_xGa_{1-x}As epitaxial layers on (1 0 0) InP for SWIR detectors. *Mater. Sci. Eng. B* 262, 114769 (2020).
 39. A.A. Bunaciu, E.G. UdrişTioiu, and H.Y. Aboul-Enein, X-ray diffraction: instrumentation and applications. *Crit. Rev. Anal. Chem.* 45(4), 289 (2015).
 40. D.C. Fu, M.S. Jusoh, A.F.A. Mat, B.Y. Majlis, XRD characterization of the MBE grown Si: GaAs, GaAs, AlGaAs, and InGaAs epilayer. ICONIP'02. Proceedings of the 9th International Conference on Neural Information Processing. Computational Intelligence for the E-Age (IEEE Cat. No. 02EX575). IEEE. 514 (2002).
 41. D. Zhou, and B.F. Usher, Deviation of the AlGaAs lattice constant from Vegard's law. *J. Phys. D Appl. Phys.* 34(10), 1461 (2001).
 42. S. Adachi, III-V ternary and quaternary compounds, *Springer Handbook of Electronic and Photonic Materials*. ed. S. Kasap, and P. Capper (Berlin: Springer, 2017), p. 1.
 43. M.K. Mahata, S. Ghosh, S. Jana, P. Mukhopadhyay, A. Bag, S. Mukulika, R.K. Dinara, S. Das, A. Chakraborty, D. Biswas, Growth and characterization of Al 0.15 Ga 0.85 As/

- GaAs pseudomorphic heterostructure by MBE. Proceedings of the 2014 IEEE Students' Technology Symposium. IEEE, 390 (2014).
44. W. Li, J. Du, L. Tang, Y. Tian, F. Xue, Q. Jiang, and S. Pan, Influence of boron doping amount on properties of ZnO: B films grown by LPCVD technique and its correlation to a-Si: H/ $\mu\text{c-Si}$: H tandem solar cells. *J. Mater. Sci. Mater. Electron.* 31, 6654 (2020).

Springer Nature or its licensor (e.g. a society or other partner) holds exclusive rights to this article under a publishing agreement with the author(s) or other rightsholder(s); author self-archiving of the accepted manuscript version of this article is solely governed by the terms of such publishing agreement and applicable law.

Publisher's Note Springer Nature remains neutral with regard to jurisdictional claims in published maps and institutional affiliations.

NEW

The power of the Web of Science™ on your mobile device, wherever inspiration strikes.

Dismiss

Learn More

Find a Match

Filters [Clear All](#)

- Web of Science Coverage
- Open Access
- Category
- Country / Region
- Language
- Frequency
- Journal Citation Reports

Refine Your Search Results

Journal of Electronic Materials Search

Relevancy

[Share These Results](#)

JOURNAL OF ELECTRONIC MATERIALS

SPRINGER , ONE NEW YORK PLAZA, SUITE 4600 , NEW YORK, United States, NY, 10004

ISSN / eISSN: 0361-5235 / 1543-186X

Science Citation Index Expanded

Current Contents Electronics & Telecommunications Collection | Current Contents Physical, Chemical & Earth Sciences | Essential Science Indicators

[Share This Journal](#) [View profile page](#)

** Requires free login.*

APPLIED ELECTRONIC MATERIALS

AMER CHEMICAL SOC , 1155 16TH ST, NW, WASHINGTON, USA, DC, 20036

ISSN / eISSN: 2637-6113

Science Citation Index Expanded

Current Contents Engineering, Computing & Technology | Essential Science Indicators

[Share This Journal](#) [View profile page](#)

** Requires free login.*

INFORMASIE NIDEM JOURNAL OF MICROELECTRONICS

ELECTRONIC COMPONENTS AND MATERIALS

[OPEN ACCESS](#)



Publisher: SOC MICROELECTRONICS, ELECTRON COMPONENTS MATERIALS-MIDEM ,
STEGNE 7, LJUBLJANA, SLOVENIA, 1000

ISSN / eISSN: 0352-9045 / 2232-6979

Science Citation Index Expanded

Essential Science Indicators

[Share This Journal](#)

[View profile page](#)

** Requires free login.*

ADVANCED ELECTRONIC MATERIALS

OPEN ACCESS

Publisher: WILEY , 111 RIVER ST, HOBOKEN, USA, NJ, 07030-5774

ISSN / eISSN: 2199-160X

Science Citation Index Expanded

Current Contents Physical, Chemical & Earth Sciences | Essential
Science Indicators

[Share This Journal](#)

[View profile page](#)

** Requires free login.*

ELECTRONIC MATERIALS LETTERS

Publisher: KOREAN INST METALS MATERIALS , KIM BLDG 6TH FLOOR, SEOCHO-DAERO 56
GIL 38, SEOCHO-GU, SEOUL, SOUTH KOREA, 137-881

ISSN / eISSN: 1738-8090 / 2093-6788

Science Citation Index Expanded

Essential Science Indicators

[Share This Journal](#)

[View profile page](#)

** Requires free login.*

TRANSACTIONS ON ELECTRICAL AND ELECTRONIC MATERIALS

Publisher: SPRINGER , ONE NEW YORK PLAZA, SUITE 4600 , NEW YORK, United States, NY,
10004

ISSN / eISSN: 1229-7607 / 2092-7592

Emerging Sources Citation Index

[Share This Journal](#)

[View profile page](#)

** Requires free login.*

JOURNAL OF MATERIALS SCIENCE: MATERIALS IN ELECTRONICS

Publisher: SPRINGER , VAN GODEWIJCKSTRAAT 30, DORDRECHT, NETHERLANDS, 3311 GZ

ISSN / eISSN: 0957-4522 / 1573-482X

Science Citation Index Expanded



Current Contents Electronics & Telecommunications Collection | Current Contents Engineering, Computing & Technology | Current Contents Physical, Chemical & Earth Sciences | Essential Science Indicators

[Share This Journal](#)

[View profile page](#)

**Requires free login.*

ACTIVE AND PASSIVE ELECTRONIC COMPONENTS OPEN ACCESS

HINDAWI LTD , ADAM HOUSE, 3RD FLR, 1 FITZROY SQ, LONDON, ENGLAND, W1T 5HF

ISSN / eISSN: 0882-7516 / 1563-5031

Emerging Sources Citation Index

[Share This Journal](#)

[View profile page](#)

**Requires free login.*

JOURNAL OF MICRO_NANOPATTERNING MATERIALS AND METROLOGY

SPIE-SOC PHOTO-OPTICAL INSTRUMENTATION ENGINEERS , 1000 20TH ST, PO BOX 10, BELLINGHAM, USA, WA, 98225

ISSN / eISSN: 1932-5150 / 2708-8340

Science Citation Index Expanded

Current Contents Electronics & Telecommunications Collection | Current Contents Engineering, Computing & Technology | Current Contents Physical, Chemical & Earth Sciences | Essential Science Indicators

[Share This Journal](#)

[View profile page](#)

**Requires free login.*

MATERIALS SCIENCE IN SEMICONDUCTOR PROCESSING

ELSEVIER SCI LTD , 125 London Wall, London, England, EC2Y 5AS

ISSN / eISSN: 1369-8001 / 1873-4081

Science Citation Index Expanded

Current Contents Electronics & Telecommunications Collection | Current Contents Engineering, Computing & Technology | Current Contents Physical, Chemical & Earth Sciences | Essential Science Indicators

[Share This Journal](#)

[View profile page](#)

**Requires free login.*



Clarivate.™ Accelerating innovation.

© 2023 Clarivate

[Legal center](#)

[Privacy notice](#)

[Cookie policy](#)

[Tanımlama Bilgisi Ayarları](#)

[Copyright notice](#)

[Help](#)

